

Ghost fringe removal techniques using Lissajous data presentation

David J. Erskine,^{1,a)} J. H. Eggert,¹ P. M. Celliers,¹ and D. G. Hicks²

¹Lawrence Livermore National Laboratory, L-487, Livermore, California 94551, USA

²Center for Micro-Photonics, Swinburne University of Technology, Hawthorn, Victoria 3122, Australia

(Received 10 December 2015; accepted 19 February 2016; published online 14 March 2016)

A VISAR (Velocity Interferometer System for Any Reflector) is a Doppler velocity interferometer which is an important optical diagnostic in shockwave experiments at the national laboratories, used to measure equation of state (EOS) of materials under extreme conditions. Unwanted reflection of laser light from target windows can produce an additional component to the VISAR fringe record that can distort and obscure the true velocity signal. Accurately removing this so-called ghost artifact component is essential for achieving high accuracy EOS measurements, especially when the true light signal is only weakly reflected from the shock front. Independent of the choice of algorithm for processing the raw data into a complex fringe signal, we have found it beneficial to plot this signal as a Lissajous and seek the proper center of this path, even under time varying intensity which can shift the perceived center. The ghost contribution is then solved by a simple translation in the complex plane that recenters the Lissajous path. For continuous velocity histories, we find that plotting the fringe magnitude vs nonfringing intensity and optimizing linearity is an invaluable tool for determining accurate ghost offsets. For discontinuous velocity histories, we have developed graphically inspired methods which relate the results of two VISARs having different velocity per fringe proportionalities or assumptions of constant fringe magnitude to find the ghost offset. The technique can also remove window reflection artifacts in generic interferometers, such as in the metrology of surfaces. © 2016 AIP Publishing LLC. [<http://dx.doi.org/10.1063/1.4943563>]

I. INTRODUCTION

The Velocity Interferometer System for Any Reflector (VISAR)¹⁻³ is an important diagnostic for shock physics and equation of state (EOS) experiments that measures the time history of Doppler shifted light reflected from shock or ramp loaded targets. The laser illumination often accesses the target through a window, rather than a free surface, to tamp the end of the target. Unwanted reflection of light from the target window, which might have an insufficient antireflection coating, can produce an additional zero velocity fringe component to the VISAR interferogram, called a ghost fringe, that can obscure the true science signal, and create a significant error in the perceived fringe phase, which is proportional to the output velocity we seek. In a worse case scenario, the ghost riddled phase is so different from the true phase that the velocity result is useless. Accurately removing this ghost artifact is thus essential for achieving high accuracy EOS measurements, especially when the science signal is only weakly reflected from the shock front in some targets, such as in a normally transparent material barely at a pressure which creates a reflecting shock.

A. Example streaked VISAR data

Figure 1(a) shows an example of a streak camera VISAR interferogram (data record) having a prominent ghost fringe artifact and (b) with the artifact removed showing only the science component of the signal. The time is displayed horizontally and fringes splayed out vertically in phase. Time

dependent Doppler velocity shifts produce proportional time dependent phase shifts [$\theta(t)$], with a velocity per fringe (VPF) proportionality inversely dependent on a chosen interferometer delay, so that the fringe per velocity (FPV) increases with increasing delay.

Panel (c) shows data taken simultaneous to (a) but with another VISAR with a smaller delay, so the phase shift for the same target velocity is smaller. The smaller science phase shift makes it more challenging to distinguish it from the stationary ghost. This is a motivation for accurately understanding how to best remove a ghost fringe.

B. Fourier method for deleting ghost

A popular method of distinguishing the ghost from science components is to take a discrete 2D-Fourier transform (FFT) of the interferogram, with the hope that the science and ghost components make separate peaks in frequency space. The fringe slope (phase vs time) is related to the frequency location of peaks in the 2D-FFT. With the slope being shallow for a short etalon, the peak separation and width occupy only a few frequency pixels. Thus there is the danger that the science and ghost peaks partially overlap so that deletion of the zero frequency peak pixels will also inadvertently delete some of the science frequencies. Thus while we find that the FFT zero frequency deletion method removes a majority of the ghost, it often does not do a perfect job.

C. Vector offset method for removing ghost

We introduce a new graphically inspired ghost removal method,⁴ “vector offset,” which we find intuitive and accurate

^{a)}Electronic mail: erskine1@llnl.gov.

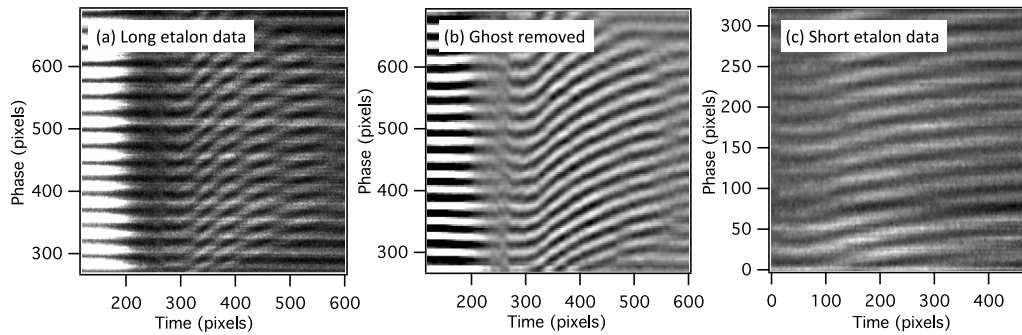


FIG. 1. ((a) and (c)) Example streak camera VISAR records having a prominent stationary artifact (ghost fringe) together with the moving science signal. The telltale “beats” in fringe magnitude (visibility) indicate presence of a ghost. These are most easily seen in the long etalon data (a) where the phase varies more strongly. Panel (b) shows (a) after ghost artifact is removed. Panel (c) shows the short etalon data measured simultaneously to the long etalon data (a), having proportionally smaller phase change vs time, so the low slope of the science fringes is more easily confused with the zero slope of the ghost fringes. This makes it more challenging to separate for the conventional method. Horizontal axes are pixels in time direction, vertical axes are y-pixels along streak camera slit direction which encode interferometer phase (and position across target). Positive velocity is downward, and the monotonic velocity change for time >300 pixels is a deceleration that follows an earlier region of positive velocity shocks, not obvious because of fringes skips and loss of visibility. The polarity of the velocity change is immaterial to the ghost removal issue. This is Omega shot s57519. Reproduced with permission from “Ghost fringe removal techniques using Lissajous data presentation,” in 19th Biennial APS Conference on Shock Compression of Condensed Matter (SCCM15), 2015, AIP Conf. Proc. (to be published). Copyright 2016 AIP Publishing LLC.⁴

for shots having mostly continuous velocity histories. (Previously, we have developed analytical equations relating net fringe magnitude to ghost amount, and these complement the graphically inspired approach here. See supplementary material of Ref. 5, Sec. D.) Figure 2 shows a vector interpretation of what happens during ghost removal. The sinusoidal portion (fringes) of the VISAR interferogram, i.e., apart from the nonfringing (NF) portion, can be expressed as a complex function $\mathbf{W}(t)$ whose real and imaginary parts represent the sine and cosine amplitudes of the sinusoidal shape for a column of the interferogram at a given time t . Equivalently, when \mathbf{W} is expressed in polar coordinates, the magnitude and phase of \mathbf{W} represents the fringe visibility and phase. A ghost component is treated as a fringe having a constant phase corresponding to zero velocity that adds vectorially to the science fringe which has a changing phase.

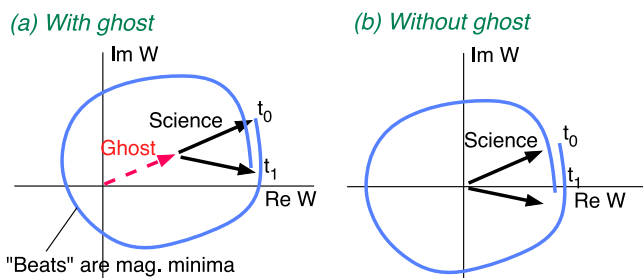


FIG. 2. How fringes of VISAR data appear when represented as a complex fringe signal $\mathbf{W}(t)$ and plotted as a Lissajous (light blue) in the complex plane, $\Im\mathbf{W}$ is plotted vs $\Re\mathbf{W}$, over some time region t_0-t_1 . (a) The two vector components (ghost, science) sum. “Beats” seen in Fig. 1 are minima in Lissajous magnitude. The vector angle is proportional to Doppler velocity, divided by the velocity per fringe proportionality VPF. The vector length is the fringe’s sinusoidal magnitude, which is proportional to the amount of coherent light reflected from the target. The ghost artifact vector (red) remains at zero velocity, while the science vector changes angle (and less strongly, magnitude) with time. (b) Removal of the ghost contribution translates the science portion so that it is recentered around the origin. Reproduced with permission from “Ghost fringe removal techniques using Lissajous data presentation,” in 19th Biennial APS Conference on Shock Compression of Condensed Matter (SCCM15), 2015, AIP Conf. Proc. (to be published). Copyright 2016 AIP Publishing LLC.⁴

D. Vector or Lissajous presentation of fringes

Various algorithms for converting fringes of a streak camera or line-VISAR to $\mathbf{W}(t)$ (i.e., phase and magnitude) are popular, including an FFT method,⁶ a sine fit along a column, and push-pull treatment of four rows at 90° .^{2,7} (The article Ref. 8 on line-imaging velocimetry, section on data reduction, is a good review.) A newer algorithm⁹ developed by the first author that compensates for Y-variation of illumination and phase, called speckle adaptive, was used to process most of the streak VISAR data here. However the ghost removal analysis described here can work with any algorithm that outputs both $\mathbf{W}(t)$ and the nonfringing intensity $NF(t)$, and all algorithms can be made to output these.

The nonfringing intensity is the vertical offset in a sine fit, or the zero frequency component in a FFT output, or the sum of the four push-pull quadrature signals. Since the NF intensity is the average value of the sinusoid, and since the bottoms of the sinusoid can never be below zero (intensity is positive), the NF intensity naturally grows when the illumination intensity or the target reflectivity grows. In the absence of any constant contribution, both the NF intensity and the magnitude of the sinusoid (i.e., size of Lissajous) will grow by the same factor. Hence the fringe magnitude and NF intensity will form a line when plotted against each other—a behavior we use fruitfully as discussed later in Sec. I G.

The complex \mathbf{W} can be represented by a vector in the complex plane. The angle of the vector (phase of the fringe) is proportional to the target Doppler velocity. This Lissajous style of data presentation was popularized by early VISARs, especially the push-pull VISAR^{2,3} which measured velocity at a single point on the target. In later years when the line- or streak camera VISARs were developed, the Lissajous presentation was not practical for displaying the change in velocity across many points along a line on the target (in which the interferometer phase also changes linearly). In that case, the raw 2D streak image was used to display the data, having the great advantage that the eye following the crest of a fringe naturally also traces out the phase or velocity profile in time.

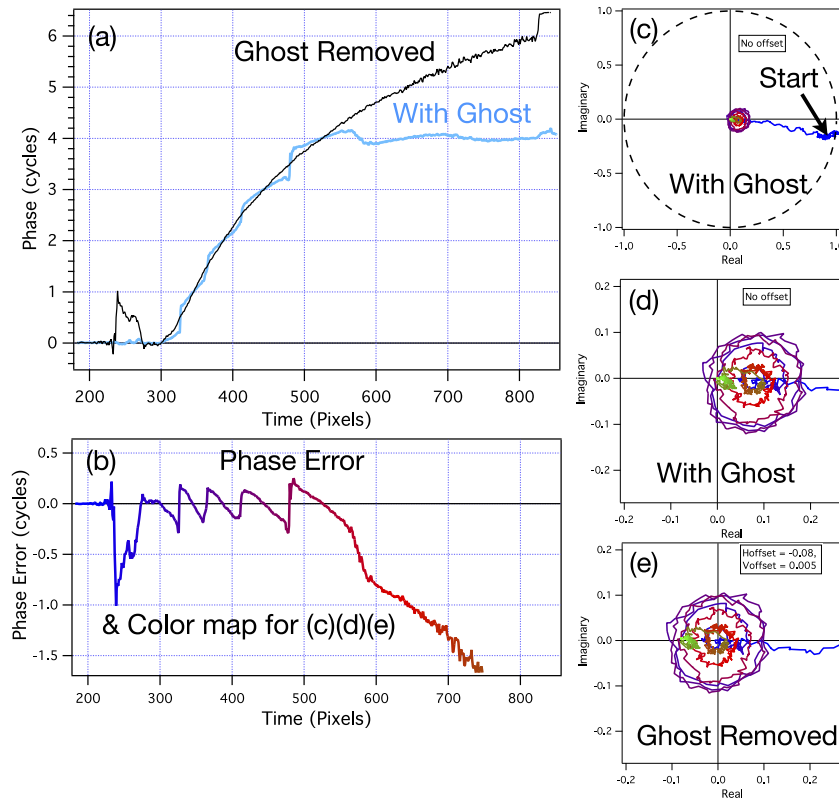


FIG. 3. (a) Phase vs time (horizontal pixels) for long etalon data of Fig. 1(a), for fringes averaged over the Y-region 380–580 pixels, for original data with ghost (blue curve), and for ghost removed by our vector offset method (black curve). ((c)–(e)) Lissajous presentation of fringes $[\mathbf{W}(t)]$, imaginary vs real parts, manifests circular loops. (b) Phase error difference between blue and black in (a). This becomes catastrophically large ($t > 550$) when the Lissajous loops of uncorrected (d) become smaller than ghost and loops no longer encompass the origin. This is solved in corrected case (e), where data are shifted by $(-0.08, 0.005)$ to center the loops. (c) Initial fringe magnitude at shock ($t = 240$) is very bright. (Integer fringe skip there in (a) has not been restored, so it is not a large phase jump). This position defines zero phase for (a) and (b). The reflected light intensity diminishes rapidly upon shock to where loops begin ($t > 300$, colored purple). Panel (b) also is a map between color and time in pixels.

However, the data analysis schemes developed for line-VISARs, such as the Fourier transform method, do not normally plot the results, even in an intermediate form, as a Lissajous. Consequently some concepts which are geometrically obvious when presented in Lissajous, such as (1) a ghost reflection will translate the science data in the 2D Lissajous space, (2) the loops of the data need to be centered over the origin for accurate phase, and (3) lopsided loops are an obvious indication of a pathology in the fringe analysis, are unfamiliar to many modern line-VISAR users. (Also, other useful associated outputs such as the magnitude and nonfringing intensity time histories are not normally outputted by Fourier transform fringe analysis packages, and thus their diagnostically useful information is often overlooked.)

In the analyses of this article, we average together several fringes in the Y-direction, giving up spatial resolution along the target for the advantage of having a single velocity history to discuss which has an improved signal to noise ratio. For those users desiring spatial resolution, one can apply the techniques described here on an individual basis to a narrow region of rows encompassing a single period in the Y-direction, and then “roll” the region upwards, recalculating it for each position to produce a Y-dependent result. This was done to produce the spatially preserved de-ghosted result of Fig. 1(b).

Both the reflection from the stationary window and the moving shock interface generate fringes, which add vectorially.

While the ghost vector remains at zero velocity, the science portion begins at zero velocity at t_0 and then evolves to other angles versus time. The initial angle θ_0 that corresponds to zero velocity is found from the data at t_0 or any time before the initial shock loading. For many figures, this has already been done so that the ghost vector lies along the horizontal axis.

The plotting of image \mathbf{W} vs real \mathbf{W} is a Lissajous plot (Fig. 2). This is a very useful presentation style for fringes, not limited to observing the ghost artifact, but includes detection of general pathologies of the fringe to $\mathbf{W}(t)$ conversion. These tend to distort the path from a circular to a lopsided shape. Figure 2(b) shows that the science signal alone $\mathbf{W}_{sci}(t)$ is a loop-like path centered at the origin. The presence of a ghost artifact \mathbf{W}_{ghst} shifts the center of the loop by a vector offset, $\mathbf{W} = \mathbf{W}_{sci} + \mathbf{W}_{ghst}$.

Therefore one can remove the ghost artifact by shifting the $\mathbf{W}(t)$ by some amount \mathbf{G}_{corr} , as $\mathbf{W} = \mathbf{W}_{sci} + \mathbf{W}_{ghst} - \mathbf{G}_{corr}$, searching until the resulting Lissajous is properly centered. We do not need to know the correction amount, it is sufficient just to center \mathbf{W} , then use this modified \mathbf{W} to compute the velocity history.

E. Example data: Effect of ghost on phase

Figures 3(a) and 3(b) show the malevolent effect of a ghost component on the perceived fringe phase for the example data

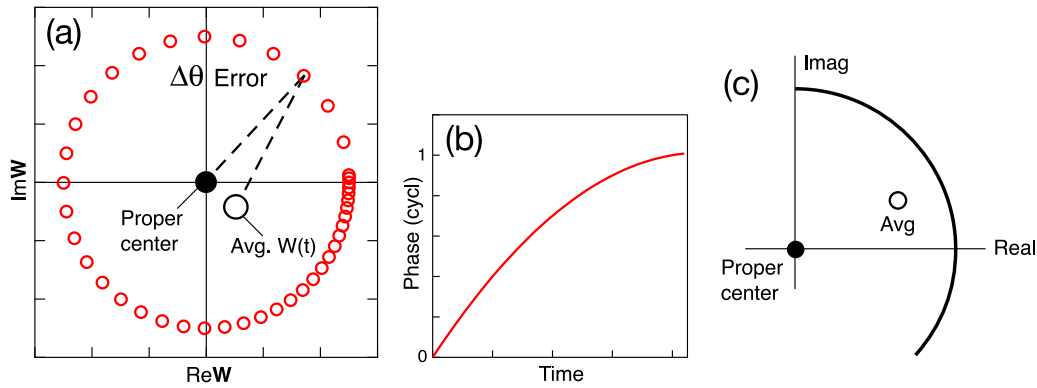


FIG. 4. (a) Example of how the average value of the Lissajous path $\mathbf{W}(t)$ (open circle), i.e., the Fourier-computed zero frequency values of the fringes, can disagree with the proper center (solid circle) if the target Doppler velocity or phase (b) has nonuniform acceleration, or if (c) the angular extent of the total phase change is not an integer number of cycles. Reproduced with permission from “Ghost fringe removal techniques using Lissajous data presentation,” in 19th Biennial APS Conference on Shock Compression of Condensed Matter (SCCM15), 2015, AIP Conf. Proc. (to be published). Copyright 2016 AIP Publishing LLC.⁴

of Fig. 1(a). Panels (c) and (d) show the off center Lissajous of the original data having ghost component, and (e) is the ghost-removed data recentered by vector offsetting. Panel (a) shows the ghosted (blue) and corrected (black) curves.

For the late time portion ($t > 550$) of the data where the reflected light from the target has diminished relative to the fixed amplitude of the ghost reflection, the loops are smaller in diameter relative to the ghost offset. Thus they miss the origin entirely, that is, they do not enclose the origin. This creates such a large phase error (b) that the perceived signal is unrelated to the true signal, and useless.

For early time ($t < 550$) when the loop diameter is larger than the ghost, so that the loop encloses the origin, the phase error is a few tenths of a cycle—large enough to be significant, but not catastrophic. Note that the phase error is periodic with the phase. This sinuous character is a commonly seen indicator of the presence of a ghost, or an incomplete removal of one because the wrong offset value was used.

F. Challenges for Fourier method for ghost deletion

An alternative and popular method is to use a 2D-FFT on the intensity image to find and then delete all near zero

frequency components in the X (time) direction, and in plus/minus “carrier” frequency in Y direction. This is equivalent to taking a 1d-FFT of the fringing signal $\mathbf{W}(t) = \mathbf{W}_{sci}(t) + \mathbf{W}_{ghst}$ and deleting the near-zero frequency components. Since \mathbf{W}_{ghst} is of zero frequency, it will certainly be removed, but the deletion process may also inadvertently remove some “good” near-zero frequency signals of $\mathbf{W}_{sci}(t)$. The presumption was that $\mathbf{W}_{sci}(t)$ does not have a large zero frequency component, and so it is not harmed. However Figs. 4 and 5 show several reasons why this is not a good presumption, especially for the short etalon VISAR which has fewer revolutions of Lissajous loops. The fewer the revolutions, the more likely \mathbf{W} has a significant nonzero average.

The FFT method of finding the zero frequency peak height is related to finding the average $\langle \mathbf{W}(t) \rangle$. So we only need to show that $\langle \mathbf{W}_{sci}(t) \rangle$ is significant to show there is a problem. For the long etalon VISAR where the Lissajous makes many loops, the average reduces toward zero. However, for the short etalon which has fewer loops, $\langle \mathbf{W}_{sci}(t) \rangle$ can be relatively significant. This can happen either when the total phase changes not an integer number of cycles (Fig. 4(c)), or when the slope of velocity vs time is nonlinear (Figs. 4(a) and 4(b)), or when the reflected intensity varies (Figure 5).

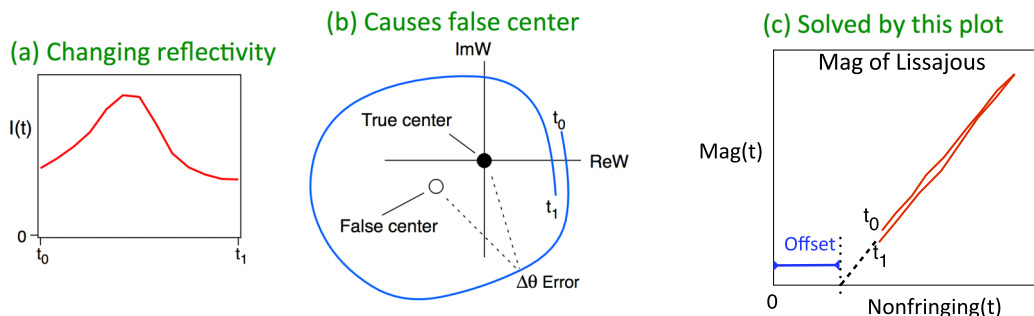


FIG. 5. (a) How the average of $\mathbf{W}(t)$ can shift due to (b) variable target reflectivity $R(t)$ that varies over a similar time that the phase changes about one cycle. This creates an apparent center not at the origin, even in the absence of a ghost reflection and when the illumination intensity is constant. The true center can be determined by plotting (c) the magnitude $|\mathbf{W}(t)|$ vs nonfringing (NF) intensity, and translating \mathbf{W} until the plot has minimized its deviation from a line or spot. This line can be offset along NF axis due to a nonfringing component of a ghost reflection, or any target incandescence or detector bias. Reproduced with permission from “Ghost fringe removal techniques using Lissajous data presentation,” in 19th Biennial APS Conference on Shock Compression of Condensed Matter (SCCM15), 2015, AIP Conf. Proc. (to be published). Copyright 2016 AIP Publishing LLC.⁴

G. Mag vs nonfringing intensity plot indicates Lissajous centration

Our solution for removing the ghost is to translate $\mathbf{W}(t)$ by a complex constant until the Lissajous loops are optimally centered. Although the latter condition can be judged approximately by eye, we have discovered that a much more accurate method is to plot Lissajous magnitude $|\mathbf{W}|$ versus the NF intensity and optimize the local linearity, which is to say we minimize the standard deviation of the data about a line or point. This method is especially more accurate than the eye when the intensity is changing with time (Fig. 5(c)), which is the usual situation. An illumination or target reflectivity change affects both the magnitude of the fringes and the non-fringing intensity by the same amount, apart from any constant contribution.

Figure 6 shows the Mag vs NF plot for the example data of Fig. 3, comparing the original (a) and de-ghosted (b) cases. By optimizing the local linearity, we do not mean the linear arrangement of the very tops of the paths associated with the Lissajous loops in the ghost-riddled case (a). Instead, we mean that those loops tighten up into small bundles as in (b), to minimize a standard deviation about some line, evaluated over the entire length of loops not just their tops.

The shock onset agrees with the dashed line but is off-screen at near (1.3,0.92) in order to enlarge the region having smaller intensity—since this is most sensitive to adjustments of the ghost offset. The late time portion beginning at the olive color is when the ghost reflection suddenly loses visibility (window destruction) and the simple constant correction becomes inappropriate. One normally deletes this section of data.

1. Minimizing sinuousness of phase also useful

For some data, especially if it is noisy, it may be difficult to determine a unique ghost amount because the Mag vs NF plot may produce linear-like shapes for several different ghost offsets. In that case, there is an additional constraint that can be used simultaneously to narrow the choice. One observes the phase vs time output as the ghost offset is varied and minimizes the degree of sinuousness. An errant offset will produce a sinuous phase error with a periodicity of integer cycles of phase, as seen in the blue curve of Fig. 3(a) where it crosses the black curve at the grid marks. Although the true phase curve is not yet known, the minds eye can detect changes about an average shape as the offset is varied. Although legitimate ripples in velocity can be seen in shockwave physics in some time regions, it is unlikely they are throughout the whole time region of the data, and unlikely to have a periodicity that is exactly commensurate to integers cycles of phase.

Note that in both methods, described in Secs. I G and I G 1, we are minimizing wiggles (sinusoidal deviations), which are either in magnitude or phase, and these two parameters correspond to the two dimensions in polar coordinates of the Lissajous. The minimization of the wiggles in magnitude is usually easier, since we have access to a curve, the nonfringing intensity, which is a good approximation to the shape of the true, nondeviated, magnitude. Whereas with the phase we do not have easy access to the true shape of the phase curve. (We

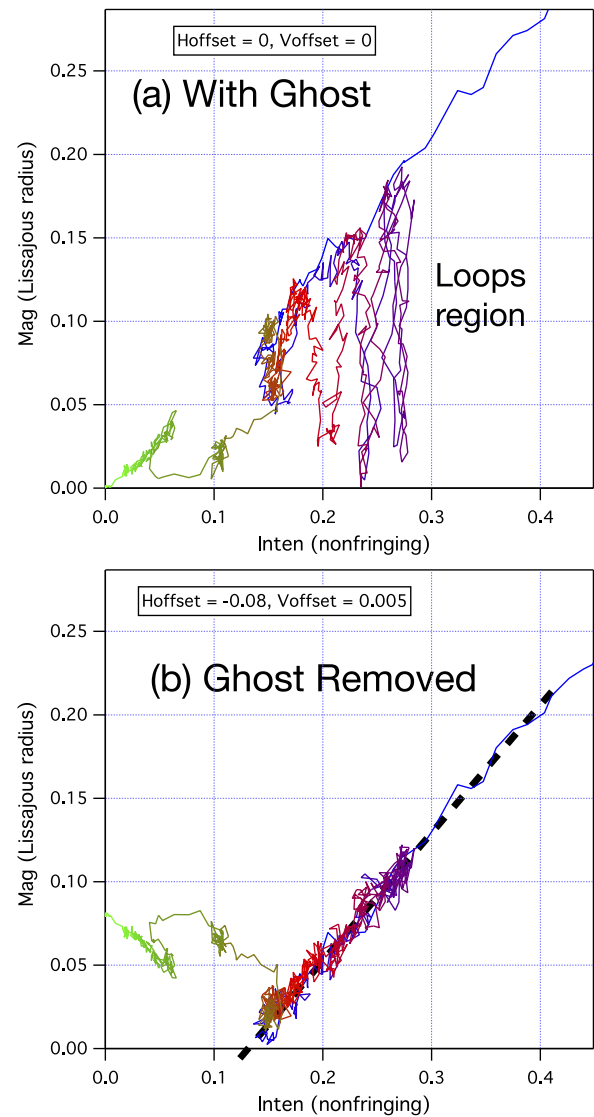


FIG. 6. Plotting Lissajous magnitude versus the nonfringing (NF) intensity is useful for gauging how centered the Lissajous loops are, especially when the NF intensity varies with time (which converts the constant magnitude of a circle into an egg shaped loop with varying magnitude). A linear relationship indicates proper centration. (a) Data of Fig. 3 having ghost; (b) after ghost removed. Shock onset is off screen at (1.3,0.92) but agrees with the dashed line. Late time portion beginning at olive color is when ghost suddenly loses visibility (window destruction) and the simple constant correction becomes inappropriate. One normally deletes this section of data.

could form it by averaging phase as we vary the ghost offset over a range—we do this with our minds eye.)

2. Semi-automatic algorithms for finding ghost offset

The optimum ghost offset is found, generally speaking, by minimizing the variance of a quantity which is either difference in magnitude or difference in phase of the data from an approximate best fit line or curve. Due to the complicated shape of the data, including the presence of noise or false features, in some cases there can be more than one minimum, and the desired minimum is not necessarily the global minimum. Therefore some human judgement is often needed. For this reason, we prefer a semi-manual approach, where the human controls the

new candidate ghost offset using a pair of slider control knobs (real and imaginary offset parts) and the computer updates all the various curves and quantities nearly instantaneously, which are displayed in plots. The human moves the two sliders until the resulting de-ghosted curves produce the best appearing result. This only takes a few seconds, so time is not a concern, and the human avoids false minima using his experience.

However, automatic algorithms can be made by straightforward programming. Rules are created to govern how an initial value for the complex offset is incremented intelligently, based on changes in the variance, so that after several iterations the variance is minimized. When the changes fall below some threshold, the search can be terminated.

II. THEORY

Equations describing the formation of fringes in an interferometer from the light of two surfaces (shock and stationary window) start with the observed intensity of light being a sum of three components

$$I(t, y) = I_{bb}(t) + Lsr(t)R(t)\{1 + \gamma \cos 2\pi[\theta(t) + \theta_0 + y]\} + Lsr(t)G\{1 + \gamma \cos 2\pi[\theta_0 + y]\}. \quad (1)$$

The first component is a constant, I_{bb} , being any target incandescence or detector bias. The next two are interferometer responses and, therefore, are proportional to the laser illumination Lsr . The middle term is due to reflection of the moving interface having reflectance R with changing science phase $\theta(t)$, and the third is due to a ghost-creating stationary window of reflectance G having stationary time-zero phase θ_0 . The y is a unit of phase proportional to the position along the streak camera slit and changes units with context. For example, $I(t, 90)$ means intensity along the interferogram row at the y position that produces 90° of interferometer output phase.

The fringing (complex) \mathbf{W} and nonfringing NF can be found by fitting a sinusoid to a vertical column (instance of time) to the data of format of Fig. 1 and assigning the cosine and sine amplitudes to the real and imaginary parts of \mathbf{W} , and the average value to NF intensity. However, for analysis, it is more useful to work with the equivalent “push-pull” equations,

$$\mathbf{W}(t) = \{[I(t, 0) - I(t, 180)] + i[I(t, 90) - I(t, 270)]\}/2, \quad (2)$$

$$NF(t) = \{I(t, 0) + I(t, 90) + I(t, 180) + I(t, 270)\}/4, \quad (3)$$

which assume that there are four phase steps at $1/4$ cycle each producing four intensity measurements $I(t, 0)$, $I(t, 90)$, $I(t, 180)$, and $I(t, 270)$. Substitution of Eq. (1) into these produces a phasor $\sim e^{i2\pi[\theta(t)+\theta_0]}$ for the science fringes, and $\sim e^{i2\pi[\theta_0]}$ for the stationary ghost.

The net corrected fringing signal is a sum of the science and ghost components minus the applied vector offset \mathbf{G}_{corr} intended to center the Lissajous and cancel the ghost. This correction does not affect the NF intensity. Hence

$$\mathbf{W} = \mathbf{W}_{sci} + \mathbf{W}_{ghst} - \mathbf{G}_{corr}, \quad (4)$$

$$NF = NF_{sci} + NF_{ghst}, \quad (5)$$

$$\mathbf{W}_{sci} = Lsr(t)R(t)\gamma e^{i2\pi[\theta(t)+\theta_0]}, \quad (6)$$

$$\mathbf{W}_{ghst} = Lsr(t)G\gamma e^{i2\pi[\theta_0]}. \quad (7)$$

The magnitude of the fringing and nonfringing signals is

$$|\mathbf{W}| = |\gamma Lsr(t)R(t)e^{i2\pi[\theta(t)+\theta_0]} + \gamma Lsr(t) \times Ge^{i2\pi[\theta_0]} - \mathbf{G}_{corr}|, \quad (8)$$

$$|\mathbf{W}_{sci}| = \gamma Lsr(t)R(t), \quad (9)$$

$$NF = [I_{bb}(t) + Lsr(t)G] + Lsr(t)R(t) \equiv NF_{Offset} + Lsr(t)R(t), \quad (10)$$

where we have collected the first two terms of NF intensity and renamed it an offset,

$$NF_{Offset} \equiv [I_{bb}(t) + Lsr(t)G]. \quad (11)$$

The γ is the instrument visibility and is ideally unity and decreases with misalignment of the optics. It can also decrease due to the velocity texture of the reflecting surface. (If the reflecting surface has a variety of Doppler shifts producing a variety of phase shifts, these wash each other out if their standard deviation is a quarter cycle or larger.)

A. Why does the Mag vs NF plot work?

In Eq. (9), the magnitude of the science fringes after we have successfully removed the ghost is $\gamma Lsr(t)R(t)$, which is proportional to the 2nd term of $NF(t)$ in Eq. (10). Hence plotting Mag vs NF intensity and removing the ghost by adjusting \mathbf{G}_{corr} will make a line of slope γ , provided that the horizontal offset NF_{Offset} is not changing with time significantly, which is an approximation.

This seems to work in practice for many shots, even though in reality the laser intensity may vary 10%–30% during the record. The key reason is that while $Lsr(t)$ may vary, it varies much slower than $R(t)$. So at each place that $R(t)$ changes rapidly, a locally linear feature is made having an approximate constant NF_{Offset} .

In a few cases with a target having several transparent layers, we had better success using multiple ghost vectors over different time periods instead of a single vector. Also, this could be a crude way of modeling a changing $Lsr(t)$. In principle, a more comprehensive analysis that models the laser intensity history with a continuous function would produce even more accurate results.

III. A MORE SUBTLE EXAMPLE

Figure 7(a) shows raw streak VISAR interferogram having a weak ghost (Omega s75265), and Fig. 9 shows its before and after correction diagrams in both Lissajous and Mag vs NF styles. This weak ghost is not obviously apparent by casually looking at interferogram, Fig. 7(a). Second, even looking at its Lissajous (Fig. 9(a)) by eye, it is not obvious where the proper center should be, since the center of the yellow loop is different than the apparent center of the greenish loop. However, the latter is just an artifact of the intensity changing with time, as easily resolved by inspecting the Mag vs NF plot, Fig. 9(b), which becomes much more linear (d) when offset by the correction (0.115, -0.03) as in (c).

The light blue to yellow mid-time region is the most important for the shock physics and we use it to optimize the

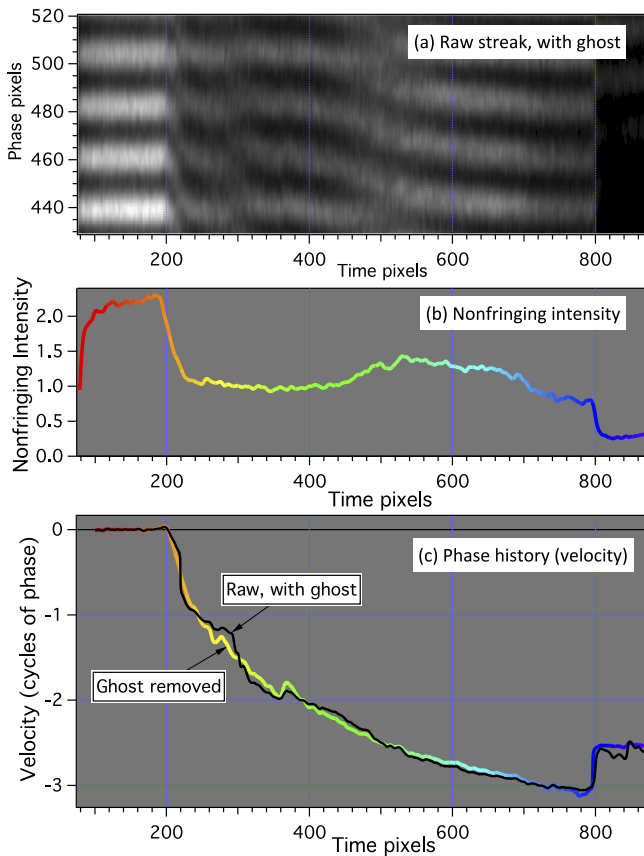


FIG. 7. (a) Streak record of Omega shot s75265 on cubic BN. Casual visual inspection of (a) does not obviously reveal the ghost. Panel (b) is nonfringing (NF) intensity. Panel (c) shows raw (black) and ghost-corrected (colored) phase vs time from (a) for rows $Y = 450\text{--}496$ (2 fringes). Note that erroneous wiggles (~ 0.25 cycle) are now absent in the colored curve. Color of curve corresponds to time. Data obtained by Amy Lazicki. Reproduced with permission from “Ghost fringe removal techniques using Lissajous data presentation,” in 19th Biennial APS Conference on Shock Compression of Condensed Matter (SCCM15), 2015, AIP Conf. Proc. (to be published). Copyright 2016 AIP Publishing LLC.⁴

correction—most of this region falls nicely into the dashed line when corrected (d). We are still speculating why the yellow and red regions have a different horizontal offset along NF axis. The purple region off the line at time 800 is the end of the sensible signal and so can be ignored.

Figure 7(c) black curve is the original velocity with the ghost, and the colored curve is with the ghost removed. Note that the black ghost-riddled curve shows significantly more wiggles than what one expects for a smoothly decaying pressure wave. Figure 8 shows the difference between these phase curves, representing the full malevolent effect of the ghost offset, as black curve.

The white “X” in Fig. 9(f) indicates the proper center of the Lissajous determined by our technique, and the white “+” as determined by the conventional method of averaging over a time region 200–800 pixels. This difference in methods would produce a phase error shown by red dashed curve in Fig. 8, indicating there is still substantial ghost effect remaining after the conventional method is applied attempting to remove it. This is as much as about 30° for the yellow time period, judged by the angle subtended by a point on the yellow portion of the curve to the X and to the +. Also, the X falls closer than the

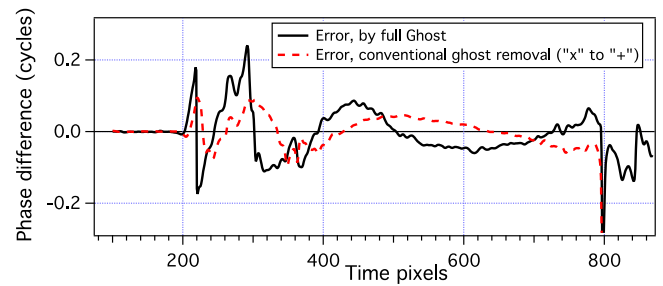


FIG. 8. Solid black curve is phase error produced by the ghost, namely, the original phase minus the de-ghosted phase in Fig. 7(c). Dotted red curve is phase error remaining after the conventional method attempts to remove it, namely, the change in phase due to Lissajous center changing between “X” and “+” in Fig. 9(c). The X is center of Lissajous according to our technique, the + is center using the average of Lissajous over time region 200–800 pixels.

+ to a line between the starting part of the Lissajous, which indicates zero phase, and the original ghosted center, marked by the white “O.”

A. Mag vs NF intensity also useful as distortion detector

This method of optimizing linearity of Mag vs NF intensity is generically useful for minimizing many other distortions of the fringing data, besides the ghost offset. These include distortions created by poor math assumptions in the algorithm converting the interferogram to $W(t)$, such as having unanticipated nonlinear phase vs Y , or uncorrected laser illumination variation vs Y . Each type of pathology produces a different kind of distortion, which deviates the Lissajous from circularity and therefore makes ripples in the Mag vs NF plot. These distortions are described further in Ref. 10 and corrected with the adjustable gains of their Eqs. 2–5 and Eqs. 10 and 11. Thus this Mag vs NF plot in Figure 5(c) is extremely useful as a general indicator of the quality of the algorithm, as applied. If a nicely linear behavior is observed, one can be confident that all these potential distortions are absent and the analysis cannot be improved further.

IV. STRATEGIES FOR DISCONTINUOUS JUMPS

We have developed strategies for computing ghost contributions for velocity profiles that have a discontinuous jump, as in Fig. 10(a). The lack of a continuous portion prevents loop-like Lissajous, making it less obvious where the proper center is. We represent the fringe state that is immediately before the jump as D_0 , defining zero phase, and immediately after the jump as D_1 and D_2 for the two VISARs systems (1 and 2).

A. Using assumption of same magnitude

Figure 10(c) shows a graphically inspired method that assumes that the relative fringe magnitudes behave the same in the two VISAR systems, so one knows that the ghost vector must be equal-distance and lie on the bisector between the two step positions D_1 and D_2 . Assuming that the initial phases at D_0 have been subtracted from the data so that the x direction

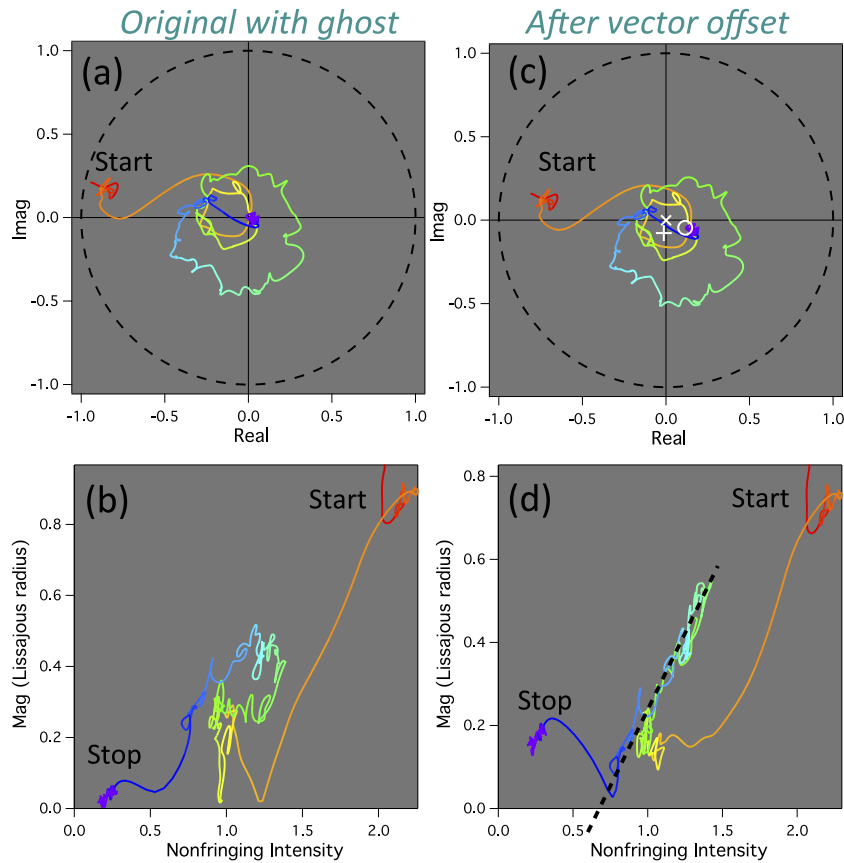


FIG. 9. (a) Yellow portion of Lissajous is off-center, and Mag vs NF plot (b) is nonlinear, indicating a ghost. Panels (c) and (d) are after ghost is removed by complex offset (0.115, -0.03). Now the Lissajous (c) is properly centered and Mag vs NF plot (d) is linear. Note blue-green and yellow portions appear not to share the same center, but that is an illusion because of intensity change for blue-green portion. (c) Original ghosted center is marked by white “O,” white “X” is Lissajous center determined by our technique, and “+” as determined by conventional method of averaging over time region 200–800 pixels. This produces a phase error $\sim 30^\circ$ for the yellow time period (angle X to + to yellow curve, see red dashes in Fig. 8). Reproduced with permission from “Ghost fringe removal techniques using Lissajous data presentation,” in 19th Biennial APS Conference on Shock Compression of Condensed Matter (SCCM15), 2015, AIP Conf. Proc. (to be published). Copyright 2016 AIP Publishing LLC.⁴

defines zero phase, then the ghost will lie along the horizontal for a length G_x . Then where the bisector intersects the horizontal axis reveals G_x . Simple algebra yields the relation

$$G_x = \frac{|D_1|^2 - |D_2|^2}{2(D_{1x} - D_{2x})}, \tag{12}$$

where we are representing the real and imaging parts of a whirl vector D by $D = D_x + iD_y$. Then we compute the science fringe phase from

$$\theta_S = \arctan \left[\frac{D_{1y}}{D_{1x} - G_x} \right]. \tag{13}$$

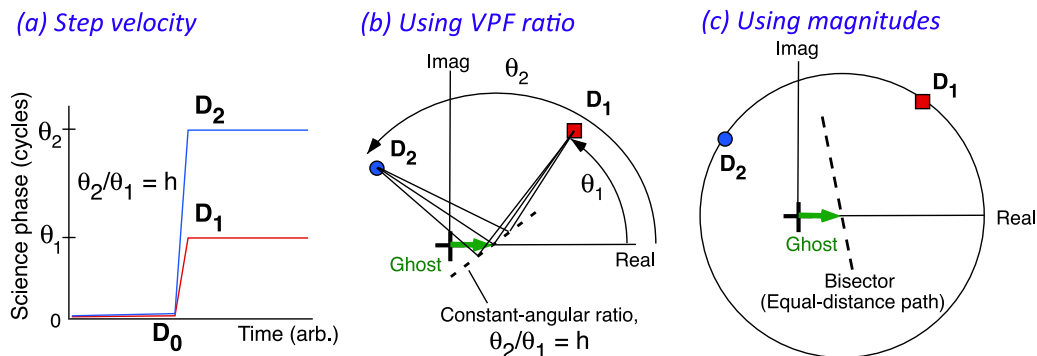


FIG. 10. (a) A discontinuous jump in velocity (phase) as in a single shock presents a different analysis challenge from the continuous phase history types. Here zero phase and hence the ghost vector (green) point along horizontal axis, but with an unknown length G_x . It is a common practice to simultaneously observe the target with two VISARs having different velocity per fringe (VPF) proportionalities. This produces a phase change in a known ratio $(VPF_1/VPF_2) = h \equiv \theta_2/\theta_1$ (ignoring integer fringe wraps). (b) In the angle ratio method, dashes satisfying a constant angular ratio intersecting the horizontal axis tell the length of the ghost vector. (c) In the same magnitude method, where relative fringe magnitude is consistent between VISARs, the ghost vector is equal-distant between D_1 and D_2 , hence where bisector intersects horizontal axis. Reproduced with permission from “Ghost fringe removal techniques using Lissajous data presentation,” in 19th Biennial APS Conference on Shock Compression of Condensed Matter (SCCM15), 2015, AIP Conf. Proc. (to be published). Copyright 2016 AIP Publishing LLC.⁴

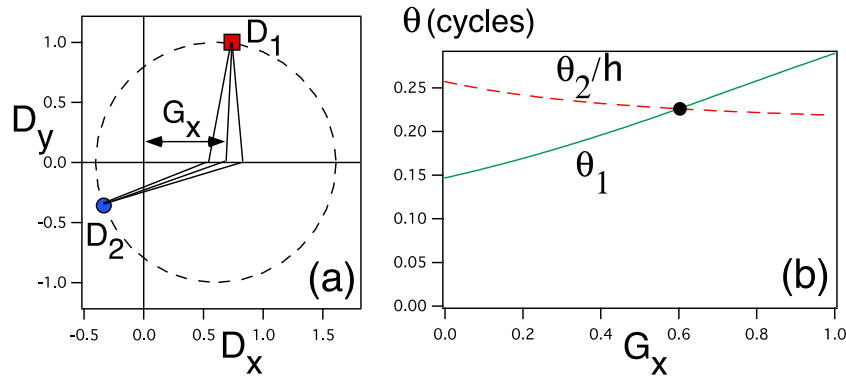


FIG. 11. The angular ratio method of Fig. 10(b) can be solved numerically by adjusting the ghost size G_x (assumed purely horizontal in (a)) until the two curves in (b) for θ_1 and θ_2/h intersect. Angles are measured from D_n to the head of ghost vector which is center of dashed circle. Zero angle is to right. Here we use simulated ghost size 0.6. The solid curve is θ_1 from Eq. (15). The dashed curve is θ_2/h from Eq. (17) with $h = 2.5$.

B. Using ratio of phase angles

Figures 10(b) and 11 show a method using prior knowledge that two different VISARs observing the same target have a ratio in their VPF proportionalities, from the ratio in the interferometer delays. Hence the angular (phase) position ratio is

$$(VPF_1/VPF_2) = h = (\theta_2 + m_2)/(\theta_1 + m_1), \quad (14)$$

where m are any integer fringe wraps. (We will ignore any fringe wraps in our example.)

The short dashed path of Fig. 10(b) is a path of constant ratio θ_2/θ_1 . Where it intersects the horizontal axis yields G_x . The governing two equations are

$$\theta_1 = \arctan \left[\frac{D_{1y}}{D_{1x} - G_x} \right], \quad (15)$$

$$\theta_2 = \arctan \left[\frac{D_{2y}}{D_{2x} - G_x} \right]. \quad (16)$$

The 2nd equation can be combined with Eq. (14) to form another function for θ_1 ,

$$\theta_1 = (1/h) \left\{ \arctan \left[\frac{D_{2y}}{D_{2x} - G_x} \right] + m_2 \right\} - m_1. \quad (17)$$

The solution to θ_1 is found by plotting the two equations, Eqs. (15) and (17), in Fig. 11(a) as two curves θ versus G_x , which ranges from 0 to 1, and finding the G_x where they intersect. Then the ghost vector is subtracted from the detected signals to reveal the science vectors $S = D - G$ where $G = G_x + i0$. Then the true fringe phase angle θ' is revealed by $\theta' = \arctan(S_y/S_x)$.

V. APPLICATIONS IN A GENERIC INTERFEROMETER

The technique can remove window reflection artifacts in other, generic interferometer diagnostics, such as in the measurement of a surface height. Consider that the spatial

variable, along any 2D-path on the surface, is analogous to the time variable of the preceding analysis. The ghost reflection component could be spatially constant, while we suppose the surface height varies along the path, the latter which could make a loop path in the Lissajous analogous to the loops discussed earlier, while the window reflection would contribute a constant value that would shift the center of that loop. As the reflected light intensity could vary from different target surface conditions, the magnitude of the surface generated fringes would grow linearly versus changes in the nonfringing intensity, analogous to the Mag vs NF plots described earlier.

ACKNOWLEDGMENTS

This work was performed under the auspices of the U.S. Department of Energy by Lawrence Livermore National Laboratory under Contract No. DE-AC52-07NA27344. Thanks to Amy Lazicki for data taking at the Omega laser facility.

¹L. Barker and K. Schuler, *J. Appl. Phys.* **45**, 3692 (1974).

²W. Hensing, *Rev. Sci. Instrum.* **50**, 73 (1979).

³D. Dolan, Sandia National Laboratory Technical Report SAND2006-1950, 2006.

⁴D. J. Erskine, J. H. Eggert, P. M. Celliers, and D. G. Hicks, "Ghost fringe removal techniques using Lissajous data presentation," in 19th Biennial APS Conference on Shock Compression of Condensed Matter (SCCM15), 2015, AIP Conf. Proc. (to be published).

⁵P. M. Celliers, P. Loubeyre, J. H. Eggert, S. Brygoo, R. S. McWilliams, D. G. Hicks, T. R. Boehly, R. Jeanloz, and G. W. Collins, *Phys. Rev. Lett.* **104**, 184503 (2010).

⁶M. Takeda, H. Ina, and S. Kobayashi, *J. Opt. Soc. Am. (1917-1983)* **72**, 156 (1982).

⁷W. M. Trott, M. D. Knudson, L. C. Chhabildas, and J. R. Asay, *AIP Conf. Proc.* **505**, 993-998 (2000).

⁸P. M. Celliers, D. K. Bradley, G. W. Collins, D. G. Hicks, T. R. Boehly, and W. J. Armstrong, *Rev. Sci. Instrum.* **75**, 4916 (2004).

⁹D. J. Erskine, "Speckle-adaptive VISAR fringe analysis technique," in 19th Biennial APS Conference on Shock Compression of Condensed Matter (SCCM15), 2015, AIP Conf. Proc. (to be published).

¹⁰D. J. Erskine, R. F. Smith, C. A. Bolme, P. M. Celliers, and G. W. Collins, *Rev. Sci. Instrum.* **83**, 043116 (2012).